Materials Today Bio 19 (2023) 100576

Contents lists available at ScienceDirect

Materials Today Bio

journal homepage: www.journals.elsevier.com/materials-today-bio

Viscoelastic hydrogels for interrogating pancreatic cancer-stromal cell interactions

Fang-Yi Lin [a], Chun-Yi Chang [b], Han Nguyen [b], Hudie Li [a], Melissa L. Fishel [c,d,e], Chien-Chi Lin [a,e,*]

[a] Department of Biomedical Engineering, Purdue School of Engineering & Technology, Indiana University-Purdue University Indianapolis, Indianapolis, IN, USA
[b] Weldon School of Biomedical Engineering, Purdue University, West Lafayette, IN, USA
[c] Department of Pediatrics, Indiana University School of Medicine, Indianapolis, IN, USA
[d] Department of Pharmacology and Toxicology, Indiana University School of Medicine, Indianapolis, IN, USA
[e] Indiana University Simon Comprehensive Cancer Center, Indianapolis, IN, USA

ARTICLE INFO

Keywords:
Hydrogels
Viscoelasticity
Pancreatic cancer
RAFT
Cancer associated fibroblasts

ABSTRACT

The tumor microenvironment (TME) is known to direct cancer cell growth, migration, invasion into the matrix and distant tissues, and to confer drug resistance in cancer cells. While multiple aspects of TME have been studied using *in vitro*, *ex vivo*, and *in vivo* tumor models and engineering tools, the influence of matrix viscoelasticity on pancreatic cancer cells and its associated TME remained largely unexplored. In this contribution, we synthesized a new biomimetic hydrogel with tunable matrix stiffness and stress-relaxation for evaluating the effect of matrix viscoelasticity on pancreatic cancer cell (PCC) behaviors *in vitro*. Using three simple monomers and Reverse-Addition Fragmentation Chain-Transfer (RAFT) polymerization, we synthesized a new class of phenylboronic acid containing polymers (e.g., poly (OEGA-*s*-HEAA-*s*-APBA) or PEHA). Norbornene group was conjugated to HEAA on PEHA via carbic anhydride, affording a new NB and BA dually modified polymer - $PEH_{NB}A$ amenable for orthogonal thiol-norbornene photopolymerization and boronate ester diol complexation. The former provided tunable matrix elasticity, while the latter gave rise to matrix stress-relaxation (or viscoelasticity). The new $PEH_{NB}A$ polymers were shown to be highly cytocompatible for *in situ* encapsulation of PCCs and cancer-associated fibroblasts (CAFs). Furthermore, we demonstrated that hydrogels with high stress-relaxation promoted spreading of CAFs, which in turns promoted PCC proliferation and spreading in the viscoelastic matrix. Compared with elastic matrix, viscoelastic gels upregulated the secretion of soluble proteins known to promote epithelial-mesenchymal transition (EMT). This study demonstrated the crucial influence of matrix viscoelasticity on pancreatic cancer cell fate and provided an engineered viscoelastic matrix for future studies and applications related to TME.

1. Introduction

Pancreatic ductal adenocarcinoma (PDAC) is a leading cause of cancer-related deaths. Early diagnosis of PDAC has been challenging owing to the complex tumor microenvironment (TME). PDAC TME is characterized by a hypovascularized stromal tissues harboring primary cancer cells, cancer-associated fibroblasts (CAFs), macrophages, other immune cells, as well as dense extracellular matrices (ECM). In particular, CAFs play a significant role in PDAC progression, including but not limited to deposition of matrices, secretion of tumor-supporting cytokines and growth factors, modulation of local immunity, and aligning matrices via cellular traction force [1]. Major ECM components secreted by CAFs include collagen, laminin, fibronectin, and hyaluronic acid (HA) [2]. The role of these components in PDAC progression have been extensively studied. For example, a recent study characterized protein compositions of normal pancreatic tissue, pancreatic intraepithelial neoplasia (PanIN), and PDAC [3] and found that basement membrane proteins laminin-511, laminin-521, and type 4 collagen were detected in normal and PanIN tissues, whereas laminin-332 and fibronectin were enriched in PDAC tissue [3]. These ECM components intercalate into a complex milieu that serves as a rich soil supporting the survival and proliferation of pancreatic cancer cells. In addition to facilitating pancreatic cancer cell progression, PDAC stroma also serves as a barrier preventing drug penetration [4]. Hence, understanding the properties of

* Corresponding author. Department of Biomedical Engineering Purdue School of Engineering & Technology Indiana University-Purdue University Indianapolis, 723 W. Michigan St. SL220K, Indianapolis, IN, 46202, USA.
E-mail address: lincc@iupui.edu (C.-C. Lin).

https://doi.org/10.1016/j.mtbio.2023.100576
Received 24 August 2022; Received in revised form 2 February 2023; Accepted 3 February 2023
Available online 4 February 2023

PDAC stromal tissue is instrumental in the development of effective treatment option against this deadly disease.

Compared with the more well-known biochemical compositions, the biophysical properties of PDAC stromal tissues are understudied. Earlier work has shown a wide variation of matrix biophysical properties in pancreatic diseases [5]. For example, the shear moduli of normal pancreatic tissue, PanIN, and PDAC tissues were characterized to be ~1.8 kPa, 2.2 kPa, and ~5 kPa. The progressively stiffer tissue along disease development was well known for different cancers. Interestingly, the stress-relaxation halftime ($\tau_{1/2}$) for normal pancreatic tissue and PDAC tissue were similar (70–80 s), whereas that of PanIN tissue was slightly faster (~20 s) [5]. Matrices with fast relaxation halftimes have great implication in cell fate processes. For example, studies have shown that faster stress-relaxation promoted mesenchymal stem cell (MSC) spreading [6], akin to the effect caused by stiff matrix. A viscoelastic surface could also redistribute vinculin to cadherin complexes in epithelial cells, leading to weakening of focal adhesion [7]. Furthermore, alginate hydrogels with faster stress-relaxation ($\tau_{1/2}$–70 s) were shown to promote lumen formation in human induced pluripotent stem cells (hiPSCs) [8]. However, alginate-based hydrogels are bio-inert and the use of divalent cations (e.g., Ca^{2+}) for alginate gel crosslinking may alter intracellular signaling.

Other than alginate hydrogels, a few other chemistries have been explored for forming hydrogels with tunable viscoelasticity, including host-guest interactions and dynamic covalent bonding. For example, Burdick and colleagues developed a hybrid hydrogel system composed of a guest-host supramolecular network and a PEG-fibrinogen covalent network [9]. In this work, the guest-host network was formed by reversible complexation between β-cyclodextrin and adamantane conjugated hyaluronic acid (HA). On the other hand, the covalent PEG-fibrinogen network was crosslinked by UV initiated chain-growth polymerization of acrylated-PEG-fibrinogen, resulting a double network structure with high tunability in matrix stiffness and tan(δ), the ratio of the loss modulus (G″) and storage modulus (G′) that characterize the dampening in the hydrogel [9]. Viscoelastic hydrogels can also be formed by incorporating dynamic covalent bonds, such as boronate ester bonding, a complex formed between boronic acid and diol moieties [10]. One benefit of hydrogels composed of boronate ester bonding is that the relaxation time can be controlled with various phenylboronic acid (BA) derivatives and a wide range of diol molecules. For example, the Anseth group integrated covalent strain promoted azide-alkyne cycloaddition (SPAAC) and reversible boronate-diol bonding to create stable hydrogels with fast relaxation time of only a few seconds ($\tau = 2\pi/\omega$ in G′-G″ crossover frequency) [11]. However, the fast relaxation time-scale (under 10 s) do not mimic pancreatic cancer tissues as noted above. In another example, Kloxin and colleagues developed co-polymer hydrogels composed of dimethylacrylamide (DMA) and pinacol protected ester of 2-acrylamidophenylboronic acid (APBA) [12]. Poly (vinyl alcohol) (PVA) was added to provide 1, 3-diols for boronate ester bond formation; however, no stress-relaxation value was provided in this study. The Cooper-White and Anseth groups synthesized photopolymerized PEG-diacrylate (PEGDA) hydrogels composed of BA-acrylate (BA-Ac) and *trans-vicinal*-diols or *cis-vicinal*-diols and showed that BA formed stronger bonding with *cis-vicinal*-diols than with *trans-vicinal*-diols [10]. In addition to using different diol molecules, different boronic acid derivatives may be used for tuning the values of tan(δ), ranging from ~0.05 to ~0.2 [10].

Boronate-diol bonding is highly desirable for forming dynamic and viscoelastic hydrogels owing to its non-toxic nature and known binding kinetics. Our group has previously reported semi-interpenetrating (semi-IPN) viscoelastic hydrogels composed of gelatin-norbornene-boronate (GelNB-BA), PEG4SH, and PVA [13,14]. The immobilized BA groups readily complexed with 1,3-diols on the entrapped PVA, resulting in hydrogels with independently tunable stiffness and stress-relaxation. However, the time scale of stress-relaxation for this gelatin-based semi-IPN hydrogels was on the order of several thousand seconds, likely due to the relatively low BA content on GelNB-BA and the lower affinity provided by 1,3-diols on PVA. We reasoned that the relaxation time scale may be decreased to the level similar to that of the PDAC matrix (<100 s) by synthesizing polymers with higher BA content and with 1,2-diols. In this work, we employed reversible addition-fragmentation chain-transfer (RAFT) polymerization to synthesize two new polymers, poly (oligo (ethylene glycol) acrylate-*s*-hydroxyethyl acrylate-*s*-acrylamidophenylboronic acid (poly (OEGA-*s*-HEAA-*s*-APBA or PEHA) and poly (HEAA)-dopamine (PHD). PEHA and PHD respectively contain tunable BA and 1, 2-diols for forming boronate ester bonds (Fig. 1). We further conjugated norbornene (NB) to PEHA via hydroxyl pendant groups on HEAA [15], rendering a $PEH_{NB}A$ macromer susceptible to orthogonal thiol-norbornene crosslinking and boronate-diol bonding. Using $PEH_{NB}A$, we designed semi-IPN hydrogels with tunable shear moduli (G') and degrees of stress-relaxation. We further used viscoelastic RAFT polymer hydrogels to study the effect of matrix mechanics on cell behaviors in pancreatic cancer associated fibroblasts (CAF) and pancreatic cancer cells (PCC), including spreading and invasion into the hydrogel matrix, gene expression, and secretory profiles.

2. Materials & methods

2.1. Materials

2-(2-Carboxyethylsulfanylthiocarbonylsulfanyl)propionic acid (CPA, 95%, Sigma-Aldrich), methanol (ACS reagent, 99.8%, Sigma-Aldrich), N,N′-diisopropylcarbodiimide (DIC, Chem-Impex), 3,4-dihydroxyphenylacetic acid (DOPAC, Ambeed), 4-dimethylaminopyridine (DMAP, Aldrich), dimethylformamide (DMF, anhydrous, Alfa Aesar), lithium phenyl-2,4,6-trimethylbenzoylphosphinate (LAP, ≥95%, Sigma-Aldrich), 4-arm thiolated PEG (PEG4SH, 10 kDa, Laysan Bio), pyridine (Fisher) were used as received. 4,4′-Azobis (4-cyanovaleric acid) (ACVA, 98%, Sigma-Aldrich) was recrystallized from methanol. Briefly, a saturated ACVA in methanol solution was prepared at room temperature. The solution was allowed to recrystallization at −20 °C overnight. The supernatant was decanted and subsequently dried in vacuum oven overnight. Oligo (ethylene glycol) methyl ether acrylate (OEGA, Mn ~ 480, Sigma-Aldrich), N-hydroxyethyl acrylamide (HEAA, 97%, Sigma-Aldrich) were passed through the inhibitor remover column for removing hydroquinone and monomethyl ether hydroquinone (Sigma-Aldrich) prior to conducting the polymerization according to manufacturer direction. 3-acrylamidophenylboronic acid (AAPBA) was obtained by reacting 3-aminophenylboronic acid with acryloyl chloride [16] (See Supporting information for details). Thiolated gelatin (GelSH) was synthesized according to Duggan et al. using gelatin, ethylene diamine, and Traut's reagent [17] (See Supporting information for details). The thiol concentration of GelSH was 0.22 mmol/g as determined by Ellman's assay.

2.2. Polymer synthesis and characterization

PHEAA, PEH, and PEHA polymers were synthesized via RAFT polymerization. For an exemplary PEHA synthesis, CPA (50 mg, 194 μmol), HEAA (1.3 g, 11.67 mmol, 60 equiv.), AAPBA (1.5 g, 7.78 mmol, 40 equiv.), OEGA (7 g, 14.58 mmol, 75 equiv.), ACVA (10.9 mg, 39 μmol, 0.2 equiv.) and methanol (19.7 g) were charged in a reaction vial with a stir bar. The reaction was purged under nitrogen for 15 min followed by reacting at 60 °C for 8 h. The product was dialyzed in regenerated cellulose (MWCO = 3.5 k) bag against pure water for 3 d and subsequently lyophilized with yield ≥90%. The feed ratio of [CTA]: [HEAA]: [AAPBA]: [OEGA]: [ACVA] was set at 1:220:0:0:0.2 for PHEAA, 1:60:0:91:0.2 for PEH, and 1:60:40:75:0.2 for PEHA, respectively. The reaction conversion and final composition was examined by ^{1}H NMR (Bruker, 500 MHz) in deuterated DMSO-d_6. Prior to molecular weight characterization by gel permeation chromatography (GPC), the boronic acid of PEHA was protected by pinacol (see supplementary information) to eliminate potential interaction between polymers and GPC columns [18]. The

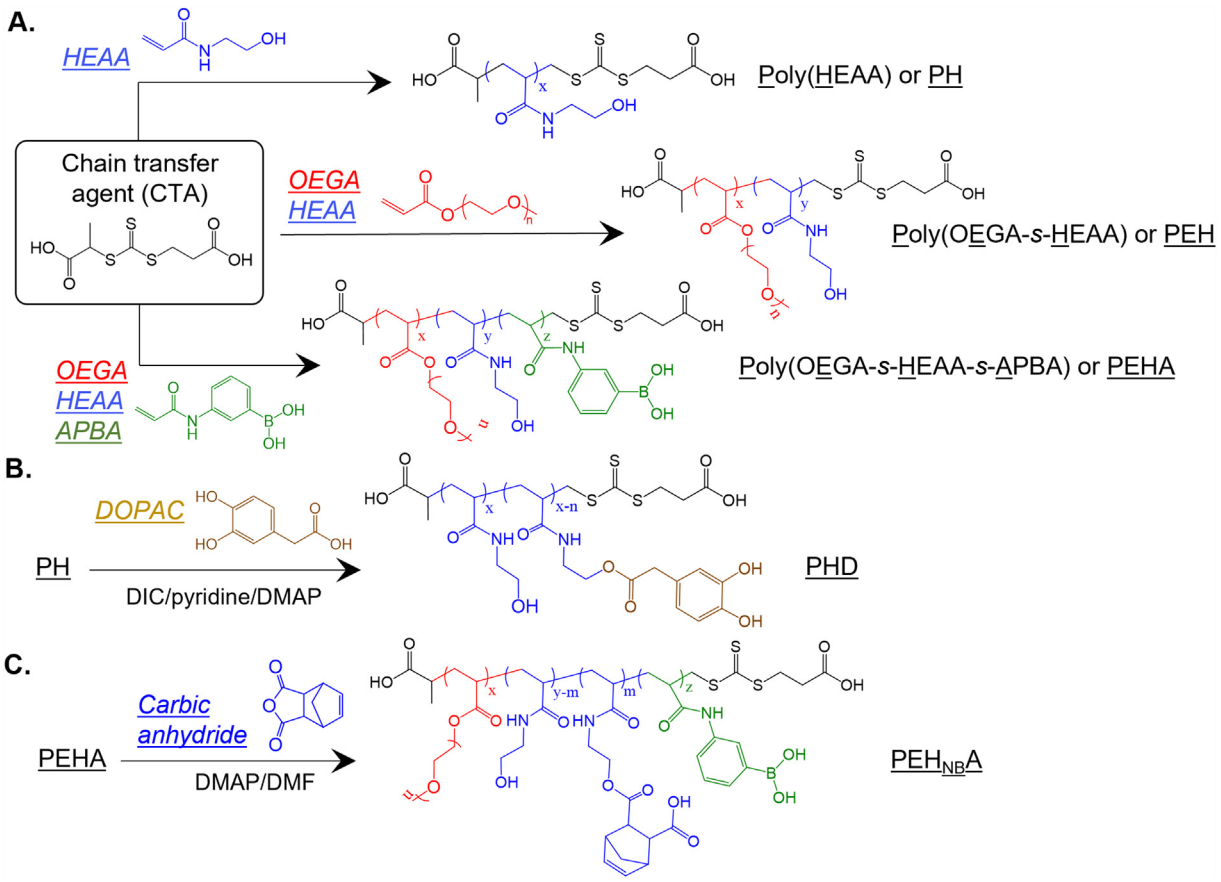

Fig. 1. Schemes of RAFT polymer synthesis. (A) RAFT polymerization for synthesis of poly (HEAA) (i.e., PH), poly (OEGA-*s*-HEAA) (i.e., PEH), and poly (OEGA-*s*-HEAA-*s*-APBA) (i.e., PEHA). (B) Conjugation of DOPAC to PH to produce 1,2-diol-containing polymer PHD. (C) Conjugation of carbic anhydride to PEHA to produce norbornene-decorated $PEH_{NB}A$.

number-average molecular weight of polymers and the corresponding dispersity were characterized by Agilent 1100 HPLC system from Cambridge Polymer Group. The system was run at 40 °C in DMF with 0.1% lithium bromide at a flow rate of 1 mL/min. The system was equipped with a UV/Vis detector and a refractive index detector, 3 Agilent PLgel Mixed-C columns and calibrated by poly (methyl methacrylate) standards. Samples were prepared at 2 mg/mL and passed through 0.45 μm PTFE filter before testing. The concentration of boronic acid in the final product of PEHA was determined by alizarin red (ARS) using protocol from Gennari et al. [19] (see supplementary information).

2.3. Conjugation of norbornene and PEH, PEHA polymers

PEH and PEHA polymers were conjugated with norbornene functional groups to afford PEH_{NB} and $PEH_{NB}A$ as the thiol-norbornene photocrosslinking macromers. Using the protocol modified from Lin and Lin [14], carbic anhydride was conjugated onto polymers through the hydroxyl groups of HEAA. Briefly, PEHA (1 g, [OH] = 1.2 mmol), carbic anhydride (0.97 g, 5.9 mmol, 5 equiv.), DMAP (73 mg, 594 μmol, 0.5 equiv.) and 10 mL DMF were combined in a reaction vial equipped with a stir bar. The reaction was conducted for 8 h at 100 °C. The product was dialyzed in pure water for 3 days and characterized by ^{1}H NMR spectra in deuterated DMSO-d_6, or deuterium oxide. The norbornene concentration was quantified by Ellman's assay (see supplementary information) as reported previously [15].

2.4. Conjugation of dopamine and PHEAA polymers

PHEAA polymers were conjugated with dopamine functional groups to enable the boronate ester chemistry in the hydrogel. Dopamine was conjugated onto PHEAA through the acid group of DOPAC and the hydrogel group of PHEAA. DOPAC (1.81 g, 10.8 mmol, 2.5 equiv.) was activated in 18 mL DMF by DIC (1.69 mL, 10.8 mmol, 2.5 equiv.) under nitrogen environment for 1 h in dark. Meanwhile, PHEAA (0.5 g, [OH] = 4.3 mmol), DMAP (263 mg, 2.2 mmol, 0.5 equiv.), and pyridine (1.74 mL, 21.5 mmol, 5 equiv.) were dissolved in 5 mL DMF. The activated DOPAC was then transferred into PHEAA solution. The reaction was continued overnight under nitrogen environment in dark. The product was dialyzed in methanol for 1 day followed by 2 days in pure water. The conjugation efficiency was analyzed by ^{1}H NMR spectra in deuterated DMSO-d_6.

2.5. Hydrogel fabrication and characterization

To crosslink hydrogels for rheological testing, PEH_{NB} (or $PEH_{NB}A$), PEG4SH, GelSH, PHD, and LAP were mixed in phosphate buffer solution (PBS) to afford final concentrations noted in each experiment. After thorough mixing, 50 μL precursor solution was pipetted on to platform of Anton Paar MCR102 rheometer for *in situ* rheometry for gelation testing (8 mm parallel plates with a gap size of 800 μm). Shear moduli data were acquired at 1 Hz with UV light ($\lambda = 365$ nm, 5 mW/cm^2) turned on at t = 60 s for a total 10 min acquisition period. The amplitude sweep and stress relaxation measurements were conducted on pre-fabricated hydrogels. That is, 60 μL precursor solution was deposited between two glass slides separated with 1 mm spacer and crosslinked under UV light ($\lambda = 365$ nm, 5 mW/cm^2) for 2 min. The hydrogels were incubated at 37 °C in PBS overnight, followed by measuring the shear moduli of hydrogels (n = 3) by amplitude sweep (8 mm plate) with a strain range of 0.1–5% at 1 Hz

and 0.25 N normal force at 25 °C. The stress relaxation curve was acquired using an initial strain of 30% for a total 15 min acquisition time. The relaxation half-time ($\tau_{1/2}$) was obtained from logarithmic plots (both X- and Y-axes) of the time-dependent relaxation curves. The scatter plot was fitted by linear or polynomial regression and the equation of the best fit was used to determine $\tau_{1/2}$, the time to reach 50% stress-relaxation (i.e., $G'/G'_0 = 0.5$).

To evaluate the effect of crosslinked gelatin (in the form of GelSH) degradation on hydrogel viscoelasticity, crosslinked hydrogels were treated with collagenase 1 for different time periods (0, 0.5, 1 h). Briefly, 100 U/mL collagenase 1 was added to the hydrogels incubated in PBS at 37 °C. Both elastic and viscoelastic hydrogels were crosslinked by 3 wt% $PEH_{NB}A$, 3 wt% GelSH, and 1 wt% PEG4SH but PHD (3 wt%) was only added to the formulations for viscoelastic hydrogels. All hydrogels crosslinking and measurement of stress-relaxation were performed as described above.

2.6. CAF & PCC encapsulation

Pancreatic cancer cells COLO-357 (a gift from Dr. Murray Korc [20,21]) were stably transduced with mKate2, a red fluorescent protein (RFP), using Incucyte® Cytolight Lentivirus reagent, followed by puromycin selection. PANC-1 cell line was obtained from ATCC. Green fluorescent protein (GFP)-labelled human pancreatic cancer associated fibroblasts (1303-GFP-49-hT, or CAF) were derived in Dr. Melissa Fishel's lab at Indiana University School of Medicine [22,23]. RFP-COLO-357, PANC-1, and GFP-CAF cells were maintained in high glucose Dulbecco's modified eagle medium (DMEM, Gibco) containing 10% Fetal bovine serum (FBS, Corning) and 1% antibiotic-antimycotic (Gibco) at 37 °C with 5% CO_2. Cells were trypsinized by 0.1% trypsin-EDTA (Gibco) for cell encapsulation. The cell density of CAF and PCC was kept at 1.6 M/mL and 400 k/mL, respectively, in both single-encapsulated and co-encapsulated precursor solutions. The hydrogel precursor solution was similar to the aforementioned formulations, except that 3 wt% of GelSH was included to facilitate cell proliferation. Before formulating into the hydrogel precursor, each component solution was sterilized by passing through 0.2 μm filter individually. Next, 25 μL of precursor solution was cured under long-wave UV light ($\lambda = 365$ nm, 5 mW/cm^2) in a cut-opened 1 mL syringe for 2 min. The cell-laden hydrogels were then cultured in regular cell culture media. Blebbistatin (40 μM, Peprotech) and ROCK inhibitor Y-27632 (10 μM, AdipoGen) were used in select experiments. The culture media was replaced daily to ensure the efficacy of inhibitors. In all cellular & molecular experiments, at least 4 hydrogels were fabricated for each group.

2.7. Cellular & molecular analyses of cell fate

Confocal images were taken on an Olympus Fluoview FV100 laser scanning microscope. Images were taken in the middle section of the gel samples, with 100 μm in total thickness at 5 μm per slice. Of note, there was no need for live cell staining as live CAFs were GFP-positive. Dead CAF cells in hydrogels were stained with ethidium homodimer 3. The cytoskeleton structure of CAF in hydrogels was visualized using F-actin (rhodamine phalloidin 100 nM, Cytoskeleton) and DAPI (1:1000, Anaspec) staining. The images were analyzed by ImageJ with FIJI package. Results included morphological analysis from at least 30 cells per condition. In the PCC/CAF co-encapsulated hydrogels, cells were stained using Actin stain 670 phalloidin (200 nM, Cytoskeleton) and DAPI (1:1000).

The invasive potential of PCC in co-encapsulated viscoelastic hydrogels was further analyzed by gene expression. On day 12, hydrogels were degraded by chymotrypsin (2 mg/mL, Worthington) treatment for cell recovery and RNA extraction. After complete gel degradation, the recovered cells were lysed for total RNA extraction using the RNA microscale kit (Thermo Fisher Scientific). 200 ng RNA of each condition was used to prepared cDNA using the cDNA synthesis kit (Thermo Fisher Scientific). Reverse transcription polymerase chain reaction (RT-PCR) was performed using the human tumor metastasis Taqman array (Thermo Fisher Scientific). Of note, the array kit contains 92 genes associated with tumor metastasis and candidate endogenous control genes, including 18 S and GAPDH. 18 S was selected as internal control for this study as it demonstrated higher stability than GAPDH for pancreatic cancer cells [24]. All primers were preloaded in the PCR plates (Table S1). Undetectable genes (CT number >40) were excluded from the analyses. Additionally, the conditioned media between day 9 and 12 was collected to investigate the secretome under different conditions. The collected media was analyzed by human growth factor antibody array C1 (RayBiotech) and human matrix metalloproteinase (MMP) antibody array C1 (RayBiotech). The membranes were imaged by LAS3000 (Fuji Film).

2.8. Statistics

All studies were repeated independently at least 3 times with each group contained at least 4 samples. Data were presented as mean ± SEM. One-way ANOVA was used to determine the statistical significance between groups. Single, double, triple, and quadruple asterisks indicate $p < 0.05$, 0.01, 0.001, and 0.0001, respectively.

3. Results

3.1. Synthesis of RAFT polymers for forming viscoelastic hydrogels

Using only three monomers, OEGA, HEAA, and APBA, three sets of RAFT polymers were synthesized – polyHEAA (i.e., PH), poly (OEGA-*s*-HEAA) (i.e., PEH), and poly (OEGA-*s*-HEAA-*s*-APBA) (i.e., PEHA) (Fig. 1A). As analyzed by ^{1}H NMR, the conversion rate of the three RAFT polymers were 90%, 81%, and 94% for PH, PEH, and PEHA, respectively (Table 1). GPC results revealed number-average molecular weights (M_n, 23.5, 35.8, and 39.6 kDa), weight average molecular weights (M_w, 34.2, 47.3, and 54.5 kDa), and dispersity (D, 1.45, 1.32, and 1.38) for PH, PEH, and PEHA, respectively (Table 1). Post-synthesis, PH was modified by DOPAC, affording dopa-conjugated polymer PHD (Fig. 1B) that provides 1,2-diols for forming boronate-ester-diol bonds with network immobilized APBA moieties. Determined by NMR spectra (Fig. S2), the conjugation efficiency DOPAC on PH was ~20%, with a Dopa concentration of 1.91 mmol/g (Table 2). PEH was used as a BA-free control polymer for BA-containing PEHA. Both PEH and PEHA were further conjugated with carbic anhydride to afford PEH_{NB} and $PEH_{NB}A$ (Fig. 1C). The later was a dually functionalized linear polymer amenable for orthogonal thiol-norbornene polymerization and boronate-ester-diol bonding. The norbornene concentration of PEH_{NB} and $PEH_{NB}A$ was quantified by a modified Ellman's assay, which determined the residual cysteine amount from the photo-click reaction between excess cysteine and norbornene in the presence of photoinitiator LAP (Supporting method). Results showed that the norbornene concentration on PEH_{NB} and $PEH_{NB}A$ was 0.40 and 0.31 mmol/g, respectively (Table 2 & Supporting method). Due to the overlap of HEAA and OEGA ester peaks at δ3.0–4.3 in NMR spectra (Fig. S3), the concentration of boronic acid in PEHA was therefore quantified by its strong complexation with 1,2,-diol containing ARS (Supporting method), which complexes with boronic acids and changes its color from red to yellow [19]. It was determined that PEHA contains 0.54 mmol/g of boronic acid (Table 2).

Table 1
GPC characterization of three RAFT polymers.

Polymer	RAFT conv.	Mn (kDa)	Mw (kDa)	Dispersity (D)
PH	90%	23.5 ± 1.12	34.2 ± 0.90	1.45 ± 0.03
PEH	81%	35.8 ± 0.65	47.3 ± 0.50	1.32 ± 0.03
PEHA	94%	39.6 ± 0.32	54.5 ± 0.22	1.38 ± 0.01

Table 2
Concentrations of DOPAC ([D]) on PHD, norbornene ([NB]) on PEHNB and $PEH_{NB}A$, and boronic acid ([BA]) on $PEH_{NB}A$.

Polymer	[D] (mmol/g)	[NB] (mmol/g)	[BA] (mmol/g)
PHD	1.91	–	–
PEH_{NB}	–	0.40	–
$PEH_{NB}A$	–	0.31	0.54

3.2. Crosslinking of synthetic viscoelastic hydrogels

The norbornene groups on PEH_{NB} or $PEH_{NB}A$ were covalently crosslinked with multi-functional thiols (e.g., PEG4SH) through thiol-norbornene photo-click reaction (Fig. 2A). Upon hydrogel crosslinking, APBA groups became pendant moieties for reversible complexation with nearby diols on PHD (Fig. 2B). Through modularly changing the macromer compositions (Fig. 2C), we prepared two groups of elastic hydrogels, one by crosslinking $PEH_{NB}A$ and PEG4SH in the absence of PHD and another by crosslinking PEH_{NB} and PEG4SH in the presence of PHD (i.e., no APBA group). In the absence of PHD (i.e., EL1), rapid crosslinking of $PEH_{NB}A$/PEG4SH hydrogels was demonstrated by *in situ* photorheometry where gel points (time for G'/G″ crossover) were found to be 8 s (EL1, Fig. 2D). Elastic hydrogels may also be crosslinked by PEH_{NB}/PEG4SH with interpenetrating PHD (EL2, gel point ~39 s. Fig. 2E). Finally, viscoelastic (VE) hydrogels were formulated by $PEH_{NB}A$, PEG4SH, and PHD (VE, gel point ~13 s. Fig. 2F). From Fig. 2F, it was apparent that the addition of PHD in $PEH_{NB}A$ hydrogels contributed to the increase of viscous moduli (G") and the corresponding tanδ (Fig. 2G). These increases were resulted from the fast equilibrium between dopamine and boronic acid functional groups, which dissipated energy when subjected to the constant strain during stress relaxation. Furthermore, changing PHD content in the precursor formulation (i.e., 0, 1, 2 wt%) resulted in hydrogels with higher elastic moduli (G', ~2.3, ~5.2, ~8 kPa, Fig. 2H) and tan(δ) (increased from ~0.02 to ~0.085, Fig. 2I), an indication that the inclusion of PHD contributed to not only the viscous but elastic properties of the hydrogels.

3.3. Evaluation of hydrogel viscoelasticity

Next, we tested the stress-relaxation of the three sets of hydrogels (i.e., $PEH_{NB}A$, PEH_{NB} + PHD, and $PEH_{NB}A$ + PHD). As shown in Fig. 3A, $PEH_{NB}A$ and PEH_{NB} + PHD (i.e., EL1 and EL2 gels) showed little relaxation and the two curves overlap with each other. On the other hand, $PEH_{NB}A$ + PHD hydrogels (i.e., viscoelastic) displayed stress-relaxation as these gels contained both boronate groups from $PEH_{NB}A$ and 1,2-diols from PHD. However, the relaxation halftime ($\tau_{1/2}$) of these VE hydrogels was about ~1500 s owing to the use of high PEG4SH content (2 wt%) that led to high hydrogel G' (~8 kPa, Fig. 2G). To further demonstrate that the stress-relaxation of $PEH_{NB}A$-based hydrogels could be tuned in a physiologically relevant range, we lowered the PEG4SH to 1 wt% and increased PHD content up to 3 wt%. Lowering PEG4SH to 1 wt % resulted in softer hydrogel with much faster stress-relaxation halftime. Specifically, the $\tau_{1/2}$ was calculated to be 30,173, 1,533, and 77 s for 1 wt %, 2 wt%, and 3 wt% PHD (Fig. 3B, Table 3), respectively, confirming the highly tunable viscoelastic nature of the $PEH_{NB}A$ semi-IPN hydrogels.

The use of orthogonal thiol-norbornene crosslinking to fabricate cell-laden hydrogels provided several benefits. First, it allowed easy adjustment of hydrogel formulations to achieve independent control of matrix stiffness and stress-relaxation. Additionally, it permitted the modular incorporation of biomimetic macromers as hydrogel crosslinker. To promote cell-matrix interactions and cell-mediated matrix remodeling, we synthesized GelSH and used it as a multifunctional thiol crosslinker to afford hydrogel crosslinking and to permit cell adhesion and protease-mediated degradation. The viscoelastic hydrogel was fabricated from 3 wt% $PEH_{NB}A$ and 3 wt% GelSH in the presence of 2 wt% PHD. It is worth noting that the addition of GelSH permitted hydrogel crosslinking while allowing cell-mediated matrix degradation critical for spreading and migration of many mesenchymal cells, including cancer-associated fibroblasts (CAFs). After photocrosslinking, the hydrogel elastic modulus was ~4.5 kPa, while tan(δ) was calculated to be 0.2 (Fig. 3C). For the elastic hydrogel, additional 0.5 wt% PEGSH along with the 3 wt% GelSH was added to the precursor solution to compensate the additional stiffening resulted from the boronate-diol bonding in the viscoelastic hydrogels. Since PEH_{NB} does not contain boronic acid for boronate ester formation, the tan(δ) of the elastic hydrogels remained low at ~ 0.02. On the other hand, tan(δ) reached over 0.2 in the viscoelastic hydrogels while maintaining G' at ~5 kPa (Fig. 3D). Additional stress-relaxation test showed that the $\tau_{1/2}$ for this specific viscoelastic hydrogel formulation was ~56 s (Fig. S4). We also evaluated the rheological properties of viscoelastic $PEH_{NB}A$ hydrogels pre-equilibrated in high glucose DMEM to gain insight into the role of glucose on the viscoelasticity of the boronic acid containing hydrogels. As shown in Fig. S5, there was no significant difference in the shear moduli and tan(δ) of viscoelastic $PEH_{NB}A$ hydrogels either equilibrated in PBS or high glucose DMEM. However, the viscoelastic hydrogels equilibrated in DMEM stress-relaxed slightly faster than that equilibrated in PBS (Fig. S6), most likely due to the presence of glucose complexes with BA groups under prolonged strain (10%, $t > 30$ s).

As the GelSH crosslinked hydrogels contained protease labile sequences, the hydrogels were subjected to collagenase 1 treatment to induce gelatin degradation. Of note, exogenously adding collagenase permitted more homogeneous gelatin degradation, enabling precise assessment of the effect of gelatin degradation on hydrogel viscoelasticity. As shown in Fig. 3E, degradation of gelatin decreased shear moduli of elastic hydrogels substantially, as GelSH was employed as a major hydrogel crosslinker. However, hydrogels crosslinked by $PEH_{NB}A$ (without PHD) and GelSH did not exhibit noticeable stress-relaxation even after 1 h of collagenase treatment (Fig. 3E, right plot). In contrast, all $PEH_{NB}A$ hydrogels crosslinked by GelSH and in the presence of PHD exhibited significant stress-relaxation (Fig. 3F). Degradation of gelatin not only decreased G', but also increased the stress-relaxation rate ($\tau_{1/2}$ decreased from ~100 s to 22 and 19 s after 0.5 h and 1 h of collagenase treatment).

3.4. Spreading of pancreatic CAFs in viscoelastic hydrogels

We next tested the cytocompatibility of the PEHA hydrogels via *in situ* encapsulation of pancreatic CAFs. Regardless of the use of PEH_{NB} or $PEH_{NB}A$ (i.e., elastic or viscoelastic hydrogel), the encapsulated CAFs remained highly viable with very limited cell death one day after *in situ* encapsulation (data not shown). After 14 days of *in vitro* culture, CAFs remained alive but with very limited spreading in elastic hydrogels (Fig. 4A – Elastic panel). In contrast, cells exhibited spindle shape morphology in viscoelastic hydrogels (Fig. 4A – Viscoelastic panel). Quantitative analyses of the cell morphology demonstrated that cells in viscoelastic hydrogels exhibited significantly lower circularity, higher aspect ratio, as well as higher cell area than that in elastic hydrogels (Fig. 4B). As CAFs are known to deposit ECM proteins to enrich the TME, we performed immunostaining of collagen and fibronectin in the CAF-laden elastic and viscoelastic hydrogels. As shown in Fig. S8, CAFs in viscoelastic hydrogels produced slightly more, but not statistically significant, collagen and fibronectin. As shown in Fig. 4C and S7, the encapsulated CAFs showed extensive spreading in the viscoelastic hydrogels. Treating CAFs with a myosin II inhibitor Blebbistatin and a ROCK inhibitor Y-27632 both disrupted F-actin polymerization (Fig. 4C). Under the influence of Blebbistatin and Y-27632, the average cell size decreased 28% and 34%, respectively (Fig. 4D) while keeping similar circularity. Blebbistatin reduced the aspect ratio slightly.

3.5. Effect of matrix viscoelasticity and CAF on PCC growth

COLO-357 cells, a pancreatic cancer cell (PCC) line derived from a

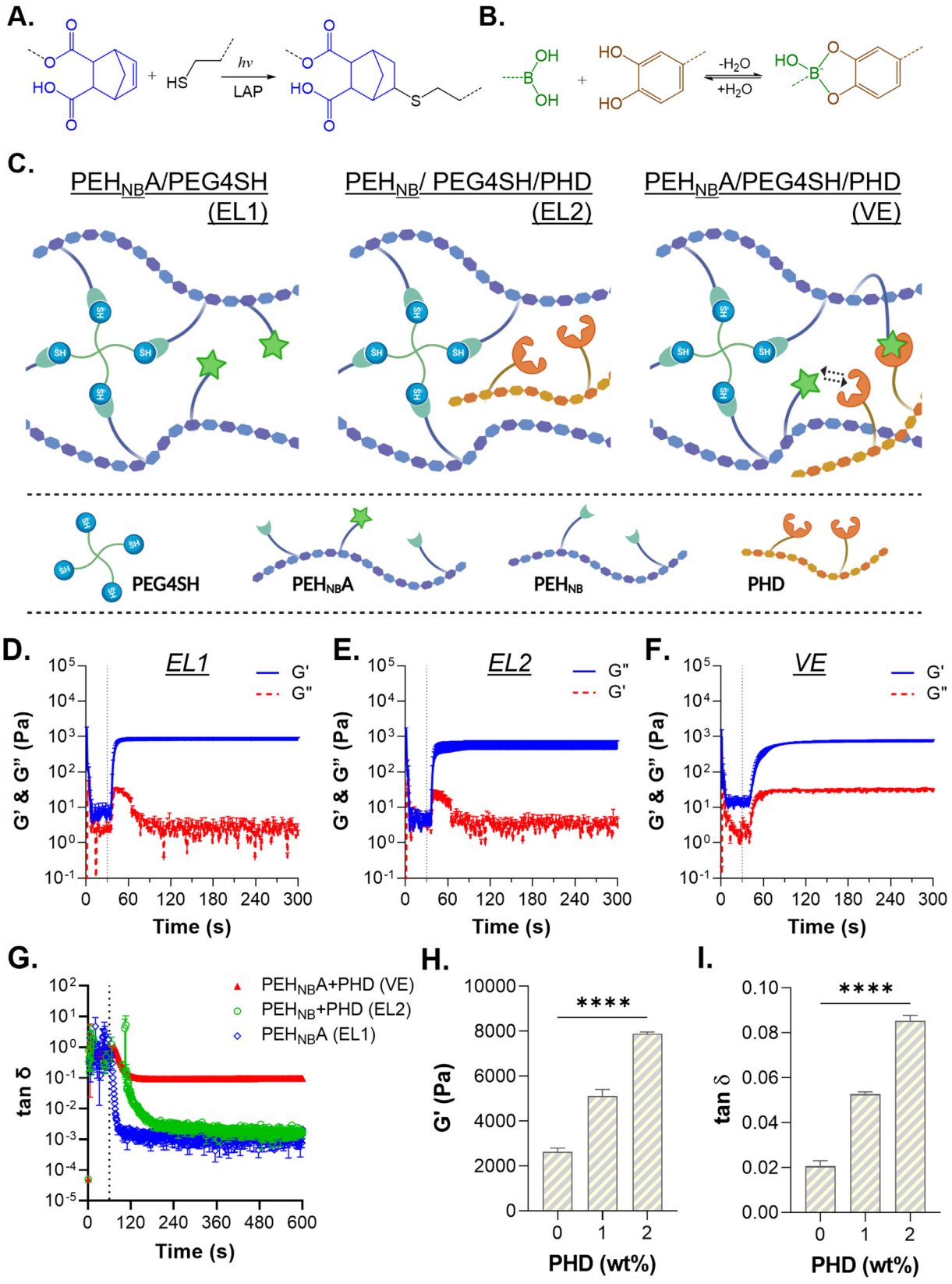

Fig. 2. Crosslinking and rheological properties of thiol-norbornene RAFT polymer hydrogels with tunable viscoelasticity. (A) Light mediated thiol-norbornene crosslinking. (B) Reversible boronate ester bonding. (C) Schematics of modular design of two elastic (EL) and one viscoelastic (VE) hydrogels (Created with BioRender.com). (D–F) In situ photo-rheometry of EL1 (D), EL2 (E), and VE (F) gels. (G) Evolution of tanδ during *in situ* photo-gelation. (H, I) Effect of PHD content on G' (H) and tanδ (I). Detailed hydrogel formulations are listed in Table 3.

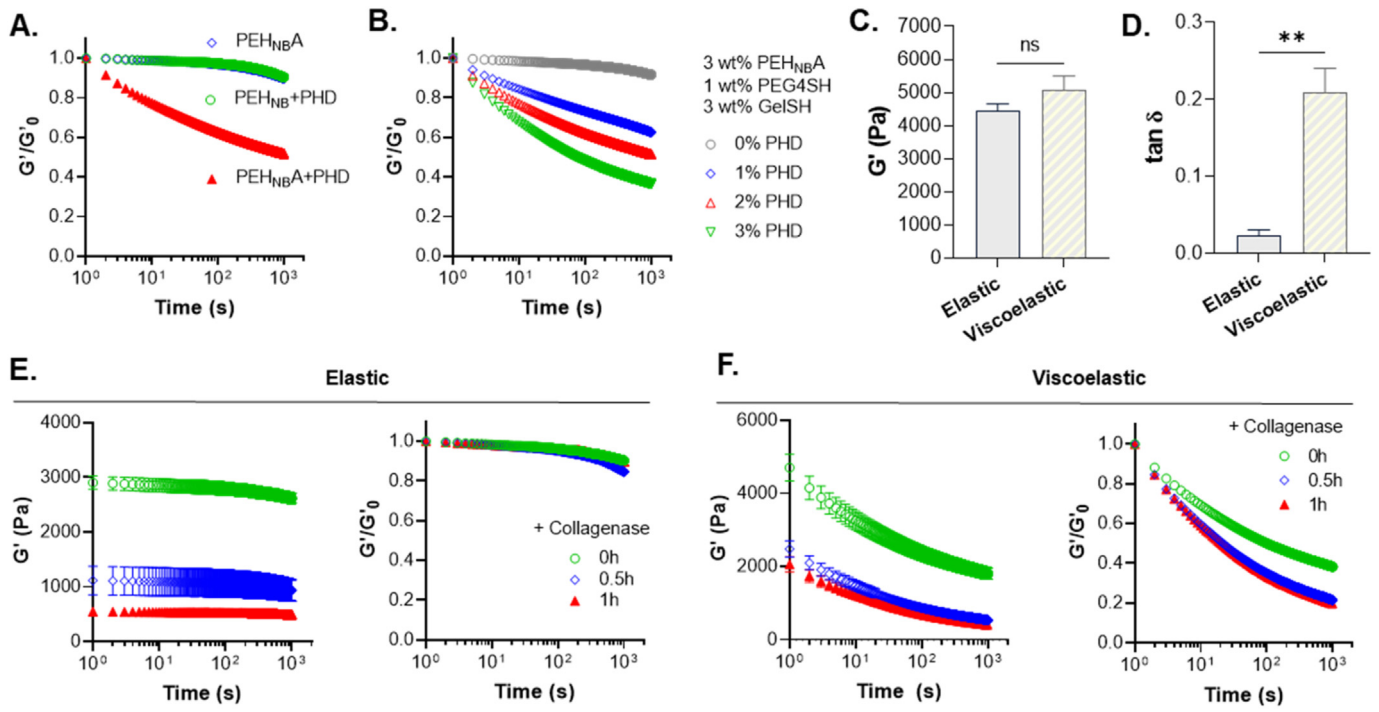

Fig. 3. Stress-relaxation of thiol-norbornene RAFT polymer hydrogels. (A) Effect of polymer compositions on stress-relaxation. (B) Effect of PHD content on stress-relaxation. (C, D) Tuning hydrogel compositions for matching shear moduli (C) with varying tan(δ) (D). Elastic gels: 3 wt% PEH_{NB}, 2 wt% PHD, 0.5 wt% PEG4SH, 3 wt% GelSH. Viscoelastic gels: 3 wt% $PEH_{NB}A$, 2 wt% PHD, and 3 wt% GelSH. Additional PEG4SH (0.5 wt%) was included in the elastic hydrogel group to ensure the two sets of gels displayed similar G'. (E, F) Effect of collagenase-mediated gel degradation of G′ and stress-relaxation (G'/G'_0) curves for elastic (E) and viscoelastic hydrogels (F). Detailed hydrogel formulations for A, B, E, F are listed in Table 3.

Table 3
Hydrogel formulations and stress-relaxation time. All polymers are in wt%. EL: Elastic, VE: Viscoelastic.

Figure	$PEH_{NB}A$	PEH_{NB}	PHD	PEG4SH	GelSH	$\tau_{1/2}$ (sec)	*Note*
2D	3	–	–	2	–	–	EL
2 E	–	3	–	2	–	–	EL
2 F	3	–	2	2	–	–	VE
2G-2I	3	–	0, 1, 2	1	–	–	VE
3 A – $PEH_{NB}A$	3	–	–	1	3	∞	EL
3 A – PEH_{NB} + PHD	–	3	2			∞	EL
3 A – $PEH_{NB}A$ + PHD	3	–	2			1567	VE
3 B	3	–	0	1	3	∞	EL
			1			30,173	VE
			2			1533	VE
			3			77	VE
3C-3D (Elastic)	3		2	1	3	∞	EL
3C-3D (Viscoelastic)	–	3				56	VE
3 F–0 h	3	–	3	1	3	103	VE
3 F–0.5 h		–				22	VE
3 F–1 h		–				19	VE

metastatic PDAC patient [25], was used to assess the effect of matrix viscoelasticity on PCC growth and potential epithelial-mesenchymal transition (EMT) in the absence or presence or CAFs. The CAF/PCC ratio was kept at 4:1 in the co-encapsulated hydrogels, which was within the range of cancer and stromal cells co-encapsulation found in recent literature [26–28]. The encapsulated PCCs showed minimal proliferation in the rather stiff (G' ~ 6 kPa) and elastic hydrogels (Fig. 5A, elastic panel), while cells in the viscoelastic hydrogels formed very small clusters after 16 days of culture (Fig. 5A, viscoelastic panel). When CAFs were co-encapsulated with PCCs in the elastic hydrogels, large PCC spheroids were visible in some area of the gels but the two cell types remained separated (Fig. 5B, elastic panel). Strikingly, when CAF and PCC cells were co-encapsulated in viscoelastic hydrogels, significant cancer cell outgrowth and irregular shapes of cell clusters were noted (Fig. 5B, viscoelastic panel). Live cell tracking of the whole gels also revealed limited cell proliferation in elastic gels but significant growth of PCC (red) in viscoelastic hydrogels (Fig. S9). Interestingly, while the addition of blebbistatin or Y-27632 significantly restricted CAF spreading in viscoelastic hydrogels, the addition of these myosin inhibitors did not alter invasive phenotype of PCC in the co-encapsulation group (Fig. 5C, separate fluorescence panels shown in Fig. S10).

Since the conditions of elastic hydrogels used in this study did not support PCC growth, we analyzed pancreatic cancer related gene expression only in cells encapsulated in viscoelastic hydrogels. TaqMan® Array Human Tumor Metastasis was used to screen for the potential molecular pathways leading to extensive spreading of PCCs in viscoelastic hydrogels in the presence of CAFs. In this study, 18 S was selected as the endogenous control gene since its expression was relatively stable (Ct values between 18.18 and 19.28) across all experimental conditions and it was a relatively more stable housekeeping genes for pancreatic

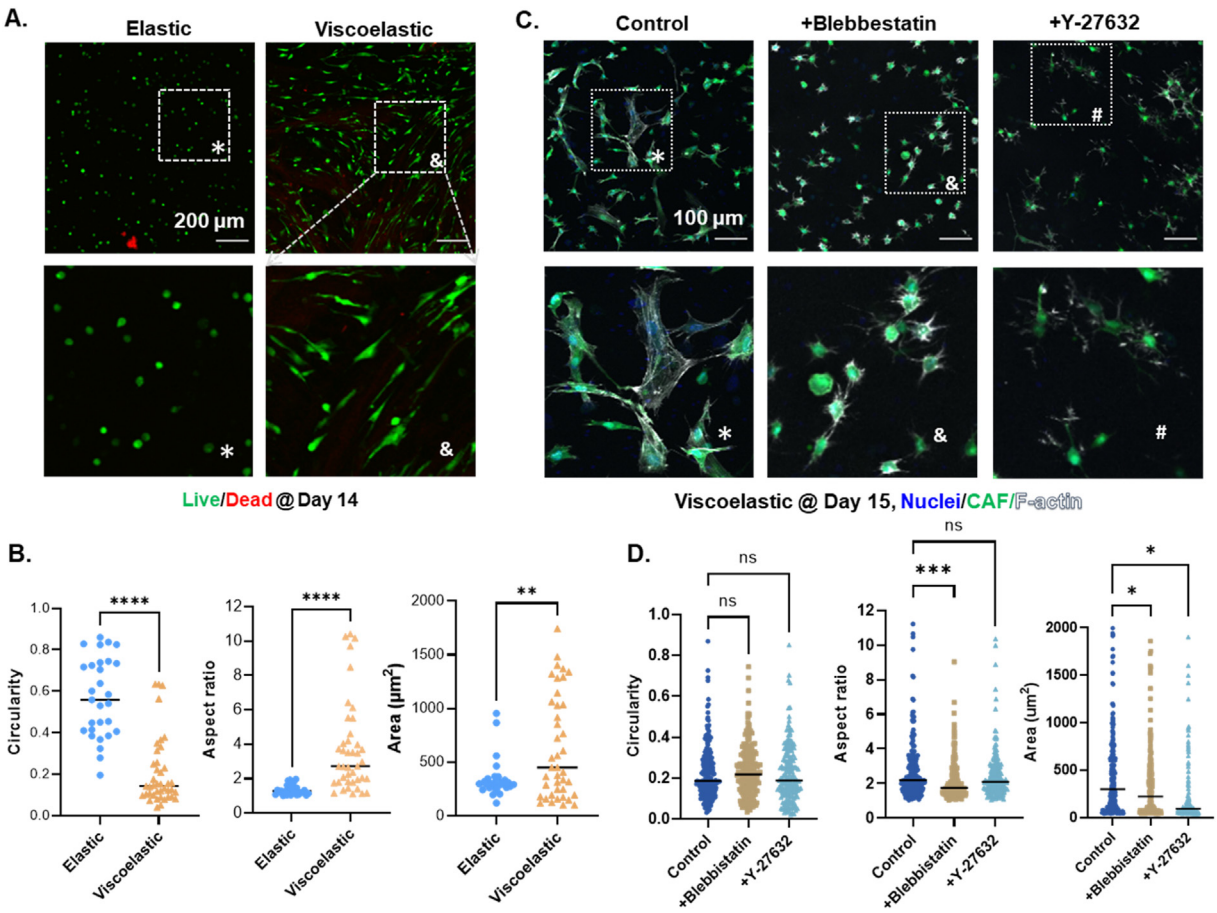

Fig. 4. Effect of matrix viscoelasticity on spreading of CAFs. (A) Live/dead staining images on Day 14. (B) Cell morphological analysis was conducted on Day 14 post-encapsulation. (C) Effect of blebbistatin and Y-27632 on inhibiting spreading of CAF in viscoelastic hydrogels (blebbistatin: 40 μM; Y-27632: 10 μM). GFP-CAFs were counter-stained with nuclei (blue) and F-actin (white). Cell morphological analysis was conducted on Day 15 post-encapsulation.

cancer cells [24]. The relative expression of all other genes was first normalized to endogenous control gene, then to the PCC only group. The expression of 92 genes between the control (PCC only) and experimental group (PCC + CAF) was organized into three groups: (1) increased expression with 2-fold or higher in the co-culture group (Fig. 5D); (2) decreased expression with 0.5-fold or lower in the co-culture group (Fig. 5E); and (3) similar expression between the two groups (data not shown). Co-culture in viscoelastic hydrogels led to significant increases in the expression of Cathepsin K (CTS), extracellular protein fibronectin (FN1), as well as various MMPs, including MMP1, MMP2, and MMP10 (Fig. 5D). Co-culture in viscoelastic hydrogels also led to significant decreases in the expression of tumor metastasis-suppressor genes NME1 [29], PNN [30], and RB1 [31], as well as protease inhibitor TIMP4 (Fig. 5E). In addition to the PCR array, we further evaluated the expression of several EMT-related genes (E-cadherin, N-cadherin, vimentin, Snail, and Zeb1) in another PCC line, PANC-1, encapsulated in elastic or viscoelastic hydrogels (Fig. S11). Compared with elastic hydrogels, cells encapsulated in viscoelastic hydrogels showed significant upregulation of E-cadherin (CDH1, 3.77-fold), N-cadherin (CDH2, 1.75-fold), vimentin (1.15-fold), SNAIL (1.43-fold), and Zeb1 (1.55-fold). Except for E-cadherin, the up-regulation of these markers were all less than 2-fold.

Multiplexed protein detection antibody arrays were used to assess conditioned media produced from CAF single culture or CAF/PCC co-culture in elastic and viscoelastic hydrogels 2 weeks after encapsulation. A total of 92 cell secreted proteins (42 cytokines, 40 inflammatory factors, and 10 MMPs/TIMPs) were detected and the protein spots were further analyzed by ImageJ to obtain semi-quantitative information about the level of secretion (Fig. 6, Fig. S12 and Fig. S13). In general, viscoelastic hydrogels promoted secretion of cytokines, inflammatory factors, and MMPs/TIMPs from both CAF single culture and CAF/PCC co-culture. Focusing on the CAF/PCC co-culture groups, numerous proteins were secreted 2-fold or higher in viscoelastic hydrogels than in elastic hydrogels, most notably HB-EGF (23.3 vs. 11.0), IGFBP-2 (100 vs. 12.9), M-CSF (21.4 vs. 10), PDGF-AA (45.6 vs. 9.5), TGF-β2 (24.3 vs. 9.5), TGF-β3 (26.7 vs. 10), MCSF-R (21.4 vs. 8.6), SCF-R (21.4 vs. 9.5), VEGF (30.1 vs. 5.2), and VEGF-R3 (21.8 vs. 10). Among these proteins, IGFBP-2, PDGF-AA, and VEGF were secreted ~5 fold or higher.

4. Discussion

Matrix stiffness and viscoelasticity are critical parameters in designing cell-laden biomaterials, as biological tissues exhibit different levels of stress-relaxation. While studies have shown that the elasticity of pancreatic stromal tissues would become progressively stiffer during pancreatic disease progression, the changes of matrix viscoelasticity (or stress-relaxation) were less studied. Rubiano *et al.* characterized the mechanical properties of resected human pancreatic tissues by indentation tesets [5]. They showed that while the steady state moduli of PDAC tumor tissues (5.46 ± 3.18 kPa) were significantly higher than that of normal tissues (1.06 ± 0.25 kPa), the differences in viscosity (η) and characteristic relaxation halftime ($\tau_{1/2}$) were similar between normal and tumor tissues (i.e., Normal tissue: η = 252 ± 134 kPa s; $\tau_{1/2}$ = 92.7 ± 46.4 s. Tumor tissue: η = 349 ± 222 kPa s; $\tau_{1/2}$ = 66.1 ± 20.8 s). On the other hand, the viscosity and stress-relaxation halftime of PanIN tissues were significantly lower than that of both normal and tumor tissues (η =

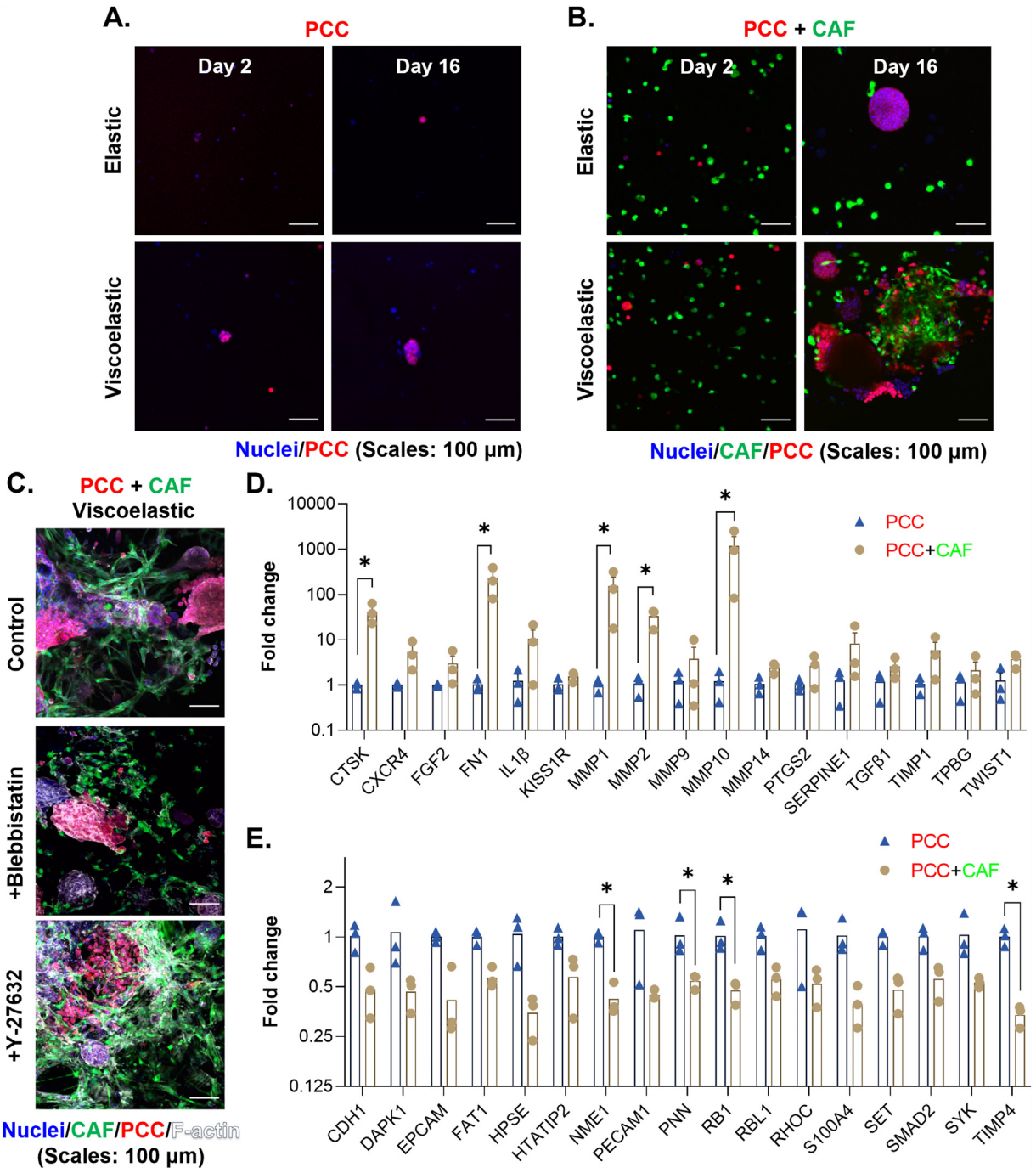

Fig. 5. Effect of matrix viscoelasticity on PCC-CAF interactions. (A) PCCs-only in elastic or viscoelastic hydrogels. (B) PCCs and CAFs co-encapsulated in elastic or viscoelastic hydrogels. (C) Effect of blebbistatin and Y-27632 on PCCs/CAFs encapsulated in viscoelastic hydrogels (blebbistatin: 40 μM; Y-27632: 10 μM). Images taken on Day 15 post-encapsulation. Images shown in separate color channels are included in Fig. S5 (D) Gene expression in PCC-only and PCC/CAF co-encapsulated viscoelastic hydrogels. (A) Upregulated and (B) downregulated genes in the co-encapsulated group.

63.2 ± 26.7 kPa s; $\tau_{1/2}$ = 27.6 ± 14.0 s). The complex mechanical properties of pancreatic tissues in different stages of disease progression warrant the development of a biomaterial system capable of decouple matrix stiffness from stress-relaxation.

Hydrogels with tunable viscoelasticity are being increasingly developed, providing a platform for understanding the complex matrix mechanics on cell fate processes. Most notably, alginate-based hydrogels have been extensively used for this purpose owing to their reversible and non-covalent ionic crosslinking [8,32–36]. Alternatively, we have reported a gelatin based semi-IPN hydrogel system to independently control matrix stiffness and viscoelasticity [13]. However, the stress-relaxation rate of the prior system was not fast enough to capture the rapid relaxation observed in biological tissues. More specifically, in our prior GelNB-BA system, we only reached relaxation halftime of about 3000 s for soft gels and 10,000 s for stiff gels. Hence, a novel design concept is needed to produce biomimetic hydrogels with highly tunable stiffness and fast stress-relaxation. Here, we designed and optimized the new viscoelastic $PEH_{NB}A$/PHD hydrogels to address the challenges associated with our prior gelatin-based viscoelastic hydrogels (GelNB--BA/PVA). While the crosslinking chemistry was the same as our prior work [12], the use of well-defined RAFT polymers affords much higher degree of control in hydrogels stiffness and stress-relaxation owing to the

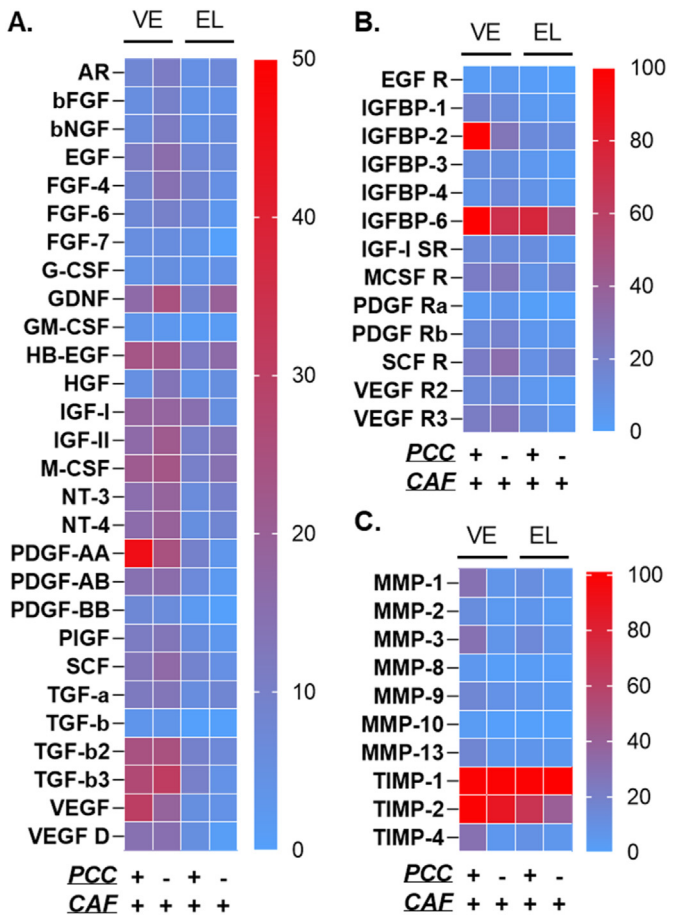

Fig. 6. Effect of hydrogel viscoelasticity on PCC/CAF secretome. (A, B) Growth factor. (C) Matrix metalloproteinase (MMPs) secreted by cells encapsulated in elastic (EL) or viscoelastic (VE). Conditioned media between day 9 and 12 were collected. Array images were shown in Fig. S12 and Fig. S13.

incorporation of higher concentration of BA groups.

To this end, we employed HEA, oEGA, and APBA to synthesize RAFT polymers with defined chemical structures and functional group concentrations. Homopolymerization of HEAA afforded PHEAA, while copolymerization of oEGA/HEAA or oEGA/HEAA/APPA produced PEH or PEHA, respectively (Fig. 1). Post-synthesis conjugation of DOPAC to PHEAAH yielded PHD, a dopamine-containing polymer that provided 1,2-diols for complexing with BA groups. On the other hand, post-synthesis modification of PEH or PEHA with carbic anhydride gave rise to PEH_{NB} or $PEH_{NB}A$, respectively. $PEH_{NB}A$ was dually functionalized polymers amenable for thiol-norbornene click gelation and boronate ester diol bonding, while PEH_{NB} was used as a control, BA-free polymer. $PEH_{NB}A$ (or PEH_{NB}) was crosslinked into hydrogels by PEG4SH (or GelSH) via light-initiated thiol-norbornene click reaction. BA groups of $PEH_{NB}A$ chains readily formed boronate-ester diols with linear PHD entrapped in the hydrogels.

We found that the inclusion of PHD delayed the gelation as dopamine on PHD is a radical scavenger that may consume radicals at the beginning of photocrosslinking. In the absence of boronate (PEH_{NB} + PHD, Fig. 2), part of the initiated radicals generated from LAP was consumed by free dopamine, resulting in slight delayed gel point (~39 s). With the use of $PEH_{NB}A$, however, dopamine groups on PHD have formed boronate ester complexes prior to photocrosslinking, leading to less free dopamine for scavenging radicals and restored the rapid thiol-norbornene photogelation (i.e., gel point ~ 13 s). Nonetheless, the advantage of this hydrogel system is on the adaptability of the polymer formulations and hydrogel viscoelastic properties (Fig. 3). For example, shear moduli of the hydrogels can be controlled by adjusting the content of PEG4SH (i.e., tuning thiol-norbornene ratio) without affecting the compositions of other macromers (i.e., $PEH_{NB}A$, PHD, or GelSH). Furthermore, the degree of hydrogel stress-relaxation may be pre-determined by synthesizing $PEH_{NB}A$ with different APBA monomer content or engineered via using PHD with different DOPAC substitution. By incorporating gelatin (in the form of GelSH) as hydrogel crosslinker, we rendered these viscoelastic hydrogels biomimetic with cell adhesive sites and were amenable to protease-mediated matrix degradation. We show that collagenase treatment led to degradation of elastic hydrogels but did not increase hydrogel stress relaxation (Fig. 3E). Collagenase-mediated degradation of viscoelastic hydrogels, however, led to simultaneous decrease in G′ and stress-relaxation half-time (Fig. 3F). These relaxation results suggest that simply degrading elastic hydrogels would not increase hydrogel stress-relaxation and that dynamic boronate ester bonding was essential for high viscoelasticity. While in this study we only explored one set of linear PEH and PEHA polymers with relatively low molecular weights (35–40 kDa), we obtained viscoelastic hydrogels with highly tunable elastic moduli (G' ~2 to 8 kPa) and relaxation halftime of (~1500–~70 s. Table 2), providing a highly adaptable platform to mimic the biophysical properties of human PDAC tumor tissue [5]. Future work may focus on synthesizing higher MW $PEH_{NB}A$/PHD that may give rise to hydrogel with ultra-high moduli and fast stress-relaxation for other biomedical applications.

Using the highly tunable RAFT polymer hydrogels, we demonstrated that high matrix viscoelasticity promoted spreading of pancreatic CAFs in 3D, whereas cell spreading in the elastic hydrogels was limited (Fig. 4). Using myosin inhibitor blebbistatin and ROCK inhibitor Y-27632, we show that CAF spreading in viscoelastic hydrogels could be partially inhibited. This result suggests that matrix viscoelasticity promoted CAF spreading with mechanisms other than the myosin and ROCK pathway. High degree of matrix stress-relaxation also promoted cancer cell growth and stromal-cancer cell interactions, as seen by the increased PCC growth and invasion phenotype (Fig. 5). Interestingly, when applying blebbistatin and Y-27632 to the PCC/CAF co-encapsulated hydrogels, these inhibitors failed to prevent CAF-induced PCC growth, suggesting that there may be other unknown biomolecular mechanisms regulating CAF-induced PCC growth. As these inhibitors did not limit cell-cell contact, the secretion of other important cytokines and growth factors by the CAFs and tumor cells was likely not affected by these inhibitors. Additional signaling and crosstalk occurring between the tumor and the CAFs could be the reason allowing the increase in PCC growth – an interesting and potentially important topic to explore in the future.

Although all hydrogels contained GelSH, a gelatin derivative susceptible to protease-mediated cleavage, PCC alone did not grow well in stiff hydrogels regardless of matrix relaxation (Fig. 5A). We attributed this to the limited use of GelSH (at 3 wt%) and relatively high matrix stiffness (G' ~ 6 kPa). The purpose of this design was to reveal the effect of matrix stress-relaxation on cell spreading and invasion into the matrix. At high gelatin content and/or soft matrix, cell spread and proliferate easily and will preclude the examination of the effect of stress-relaxation on cell fate. Although limited CAF-PCC interaction was observed in elastic hydrogels, PCCs were able to form larger spheroids (Fig. 5B), which could be a result of increasing paracrine signaling between CAFs and PCCs. Particularly, growth promoting cytokines IGF-1 and PDGF-AA were secreted more in elastic PCC/CAF co-culture condition (Fig. 6A). On the other hand, PCC proliferation and invasion were significantly promoted in viscoelastic hydrogels when CAFs were co-encapsulated (Fig. 5B and C). When both cell types were co-encapsulated in viscoelastic hydrogels, close interactions between PCCs and CAFs were notable, with PCCs exhibiting invasive phenotype (Fig. 5B and C). The phenotypic changes of PCCs/CAFs were corroborated by significant increases in mRNA expression of protease Cathepsin K (CTSK), cell-adhesive protein fibronectin 1 (FN1) and MMPs (MMP-1, 2, 10) (Fig. 5D). Both CTSK and MMPs are implicated in matrix degradation, while FN1 was increasingly deposited in tumor tissues. Furthermore,

many genes implicated in tumor and metastasis suppression also down-regulated in PCC/CAF co-cultured in viscoelastic gels (e.g., NME1, PNN, RB1, Fig. 5E). While in this work we demonstrated some level of EMT marker expression in viscoelastic hydrogels, a recent work reported by Ruiter *et al.* demonstrated that stress-relaxing alginate-based hydrogels down-regulated EMT associated proteins in kidney organoids [37]. Additional studies are needed to obtain conclusive results on the effect of matrix stress-relaxation on pancreatic cancer cells.

Since elastic hydrogels did not induce PCC invasive phenotype even in the presence of CAFs, we hypothesized that high matrix viscoelasticity likely promoted secretion of cytokines and other proteins that then induced PCC invasion into the matrix. In a recent study, silk-based hydrogels with stress-relaxing properties were used to culture MSCs. The expression of apolipoprotein, MIF, thrombospondin, osteopontin, VEGF, IL-8, PDGF-AB/BB, IGFBP-2, and VCAM-1 were upregulated in viscoelastic silk hydrogels [38]. In this study, the secretion of many growth- and EMT-promoting cytokines were promoted from PCC/CAF co-culture in viscoelastic hydrogels (e.g., HB-EGF, PDGF-AA, TGF-β2, TGF-β2, and IGFBP-2. Fig. 6A and B). Of note, overexpression of TGF-β2 in pancreatic cancer has been linked to immunosuppression, metastasis, angiogenesis, and proliferation [39]. Furthermore, growing evidence indicates that IGFBP-2 in cancer cells is a "hub" for an oncogenic network [40], which connects multiple cancer signaling pathways. For example, IGFBP-2 activates the NF-κB pathway to drive EMT and invasive phenotype in PDAC [41]. IGFBP-2 also promotes tumor progression by inducing alternative polarization of macrophages in PDAC through the STAT3 pathway [42]. Co-culture also promoted the secretion of VEGF, and VEGF-R3, as well as proteases responsible for matrix degradation (MMP-1, 2, 3, 9, 13, Fig. 6C), a prerequisite for cell spreading and invasion. Of note, both TIMP-1 and TIMP-2 were overexpressed in PDAC tissues [43]. While the major function of TIMPs is to inhibit MMPs, their expression is typically coordinated with the level of proteases. It was also hypothesized that the production of inhibitors may be a cellular reaction to the increased presence of proteases. Upregulation of TIMP-1 mRNA expression was correlated with aggressive tumors and our results corroborated with the literature. Moreover, high levels of TIMP-1 or TIMP-2 protein have been associated with poor prognosis. On the other hand, TIMP-2 may be growth-stimulating or growth-inhibiting, depending on their concentrations and the cell types [43].

5. Conclusion

We have designed a linear acrylate/acrylamide copolymer platform that contains norbornene and boronic acid moieties for hydrogel fabrication. The fabrication of synthetic semi-IPN hydrogels was through thiol-norbornene photocrosslinking chemistry and boronate ester equilibrium between phenylboronic acid and dopamine. This synthetic hydrogel system allows independent control of the stiffness and viscoelasticity (or stress relaxation). The hydrogel stiffness and viscoelasticity were carefully regulated to mimic the pancreatic tumor microenvironment at elastic modulus ~6 kPa with or without stress relaxation characteristic for pancreatic cancer cells COLO-357 and pancreatic cancer-associated fibroblasts cell encapsulation. At this condition, we found out that CAFs only spread in viscoelastic hydrogels while kept the circular shape in the elastic hydrogels. The encapsulated PCC cells showed minimal proliferation. However, CAF facilitated the proliferation of PCC in both elastic and viscoelastic hydrogels during co-encapsulation. While the two cell types remained intact in elastic condition, irregular cell clusters with outgrowing cancer cells were found in the viscoelastic condition. This cell behavior implied that high matrix viscoelasticity may contribute to tumor metastasis *in vivo*. We further investigated the interactions between cells in viscoelastic hydrogels by gene expression and cytokine secretion. The results suggest that one potential mechanism for PCCs to exhibit invasive phenotype was by significantly increasing cell-adhesive protein (FN1) along with aggressively degrading hydrogel matrix (MMP-1, 2, 10), while downregulated tumor and metastasis suppression (NME1, PNN, RB1). The investigation of secretome further identified several cytokines, inflammatory factors, and MMPs that may promote PCC invasion into the matrix. The large increase in pression of IGFBP-2, PDGF-AA, VEGF and various MMPs (MMP-1, 2, 3, 9, 13) indicated cell spreading and invasion of co-encapsulated cells in viscoelastic hydrogel. To best of our knowledge, this is the first study that demonstrates extensive cancer cell invasion assisted by cancer-associated fibroblasts can be regulated by hydrogel viscoelasticity. This system has the potential to serve as the *in vitro* model for screening and testing anticancer drugs.

Credit author statement

Fang-Yi Lin: Data curation; Formal analysis; Investigation; Methodology; Validation; Writing – original draft, review & editing. **Chun-Yi Chang:** Data curation; Formal analysis. **Han Nguyen:** Data curation; Formal analysis. **Hudie Li**, Data curation; Formal analysis. **Melissa L Fishel**: Funding acquisition; Resources; Writing – review & editing. **Chien-Chi Lin**: Conceptualisation; Investigation; Funding acquisition; Resources; Supervision; Writing – review & editing.

Declaration of competing interest

The authors declare the following financial interests/personal relationships which may be considered as potential competing interests: Chien-Chi Lin reports financial support was provided by National Institutes of Health. Melissa Fishel reports financial support was provided by National Institutes of Health. Chien-Chi Lin has patent pending to Indiana University.

Data availability

Data will be made available on request.

Acknowledgement

This work is supported by the National Cancer Institute (R01CA227737, to C.-C.L. R01CA167291, R01CA211098 to M.L.F).

Appendix A. Supplementary data

Supplementary data to this article can be found online at https://doi.org/10.1016/j.mtbio.2023.100576.

References

[1] E. Hessmann, S.M. Buchholz, I.E. Demir, S.K. Singh, T.M. Gress, V. Ellenrieder, A. Neesse, Microenvironmental determinants of pancreatic cancer, Physiol. Rev. 100 (4) (2020) 1707–1751.
[2] A. Neesse, C.A. Bauer, D. Öhlund, M. Lauth, M. Buchholz, P. Michl, D.A. Tuveson, T.M. Gress, Stromal biology and therapy in pancreatic cancer: ready for clinical translation? Gut 68 (1) (2019) 159–171.
[3] C.R. Below, J. Kelly, A. Brown, J.D. Humphries, C. Hutton, J. Xu, B.Y. Lee, C. Cintas, X. Zhang, V. Hernandez-Gordillo, A microenvironment-inspired synthetic three-dimensional model for pancreatic ductal adenocarcinoma organoids, Nat. Mater. (2021) 1–10.
[4] R. Alzhrani, H.O. Alsaab, K. Vanamala, K. Bhise, K. Tatiparti, A. Barari, S. Sau, A.K. Iyer, Overcoming the tumor microenvironmental barriers of pancreatic ductal adenocarcinomas for achieving better treatment outcomes, Adv. Ther. 4 (6) (2021), 2000262.
[5] A. Rubiano, D. Delitto, S. Han, M. Gerber, C. Galitz, J. Trevino, R.M. Thomas, S.J. Hughes, C.S. Simmons, Viscoelastic properties of human pancreatic tumors and in vitro constructs to mimic mechanical properties, Acta Biomater. 67 (2018) 331–340.
[6] K. Dey, S. Agnelli, L. Sartore, Dynamic freedom: substrate stress relaxation stimulates cell responses, Biomater. Sci. 7 (3) (2019) 836–842.
[7] J.Y. Zheng, S.P. Han, Y.-J. Chiu, A.K. Yip, N. Boichat, S.W. Zhu, J. Zhong, P. Matsudaira, Epithelial monolayers coalesce on a viscoelastic substrate through redistribution of vinculin, Biophys. J. 113 (7) (2017) 1585–1598.
[8] D. Indana, P. Agarwal, N. Bhutani, O. Chaudhuri, Viscoelasticity and adhesion signaling in biomaterials control human pluripotent stem cell morphogenesis in 3D culture, Adv. Mater. 33 (43) (2021), 2101966.

[9] C. Loebel, A. Ayoub, J.H. Galarraga, O. Kossover, H. Simaan-Yameen, D. Seliktar, J.A. Burdick, Tailoring supramolecular guest-host hydrogel viscoelasticity with covalent fibrinogen double networks, J. Mater. Chem. B 7 (10) (2019) 1753–1760.
[10] I.A. Marozas, K.S. Anseth, J.J. Cooper-White, Adaptable boronate ester hydrogels with tunable viscoelastic spectra to probe timescale dependent mechanotransduction, Biomaterials 223 (2019), 119430.
[11] S. Tang, H. Ma, H.C. Tu, H.R. Wang, P.C. Lin, K.S. Anseth, Adaptable fast relaxing boronate-based hydrogels for probing cell-matrix interactions, Adv. Sci. 5 (9) (2018), 1800638.
[12] M.E. Smithmyer, C.C. Deng, S.E. Cassel, P.J. LeValley, B.S. Sumerlin, A.M. Kloxin, Self-healing boronic acid-based hydrogels for 3D co-cultures, ACS Macro Lett. 7 (9) (2018) 1105–1110.
[13] H.D. Nguyen, X. Sun, H. Yokota, C.-C. Lin, Probing osteocyte functions in gelatin hydrogels with tunable viscoelasticity, Biomacromolecules 22 (3) (2021) 1115–1126.
[14] M.H. Kim, H. Nguyen, C.-Y. Chang, C.-C. Lin, Dual functionalization of gelatin for orthogonal and dynamic hydrogel cross-linking, ACS Biomater. Sci. Eng. 7 (9) (2021) 4196–4208.
[15] F.-Y. Lin, C.-C. Lin, Facile synthesis of rapidly degrading PEG-based thiol-norbornene hydrogels, ACS Macro Lett. 10 (3) (2021) 341–345.
[16] M. Chen, Y. Lu, Q. Ma, L. Guo, Y.-Q. Feng, Boronate affinity monolith for highly selective enrichment of glycopeptides and glycoproteins, Analyst 134 (10) (2009) 2158–2164.
[17] S. Duggan, O. O'Donovan, E. Owens, W. Cummins, H. Hughes, Synthesis of mucoadhesive thiolated gelatin using a two-step reaction process, Eur. J. Pharm. Biopharm. 91 (2015) 75–81.
[18] Y. Zhong, B. Song, D. He, Z. Xia, P. Wang, J. Wu, Y. Li, Galactose-based polymer-containing phenylboronic acid as carriers for insulin delivery, Nanotechnology 31 (39) (2020), 395601.
[19] A. Gennari, C. Gujral, E. Hohn, E. Lallana, F. Cellesi, N. Tirelli, Revisiting boronate/diol complexation as a double stimulus-responsive bioconjugation, Bioconjugate Chem. 28 (5) (2017) 1391–1402.
[20] J. Kleeff, K. Fukahi, M.E. Lopez, H. Friess, M.W. Büchler, B.A. Sosnowski, M. Korc, Targeting of suicide gene delivery in pancreatic cancer cells via FGF receptors, Cancer Gene Ther. 9 (6) (2002) 522–532.
[21] K. Matsuda, T. Idezawa, X.J. You, N.H. Kothari, H. Fan, M. Korc, Multiple mitogenic pathways in pancreatic cancer cells are blocked by a truncated epidermal growth factor receptor, Cancer Res. 62 (19) (2002) 5611–5617.
[22] K.E. Richards, A.E. Zeleniak, M.L. Fishel, J. Wu, L.E. Littlepage, R. Hill, Cancer-associated fibroblast exosomes regulate survival and proliferation of pancreatic cancer cells, Oncogene 36 (13) (2017) 1770–1778.
[23] C.Y. Chang, H.C. Johnson, O. Babb, M.L. Fishel, C.C. Lin, Biomimetic stiffening of cell-laden hydrogels via sequential thiol-ene and hydrazone click reactions, Acta Biomater. 130 (2021) 161–171.
[24] W.L. Ge, G.D. Shi, X.M. Huang, Q.Q. Zong, Q. Chen, L.D. Meng, Y. Miao, J.J. Zhang, K.R. Jiang, Optimization of internal reference genes for qPCR in human pancreatic cancer research, Transl. Cancer Res. 9 (4) (2020) 2962–2971.
[25] R. Morgan, L. Woods, G. Moore, L. Quinn, L. McGavran, S. Gordon, Human cell line (COLO 357) of metastatic pancreatic adenocarcinoma, Int. J. Cancer 25 (5) (1980) 591–598.
[26] F.L. Lai Benjamin, X. Lu Rick, Y. Hu, H.L. Davenport, W. Dou, E.Y. Wang, N. Radulovich, M.S. Tsao, Y. Sun, M. Radisic, Recapitulating pancreatic tumor microenvironment through synergistic use of patient organoids and organ-on-a-chip vasculature, Adv. Funct. Mater. 30 (48) (2020).
[27] H. Saini, K. Rahmani Eliato, J. Veldhuizen, A. Zare, M. Allam, C. Silva, A. Kratz, D. Truong, G. Mouneimne, J. LaBaer, R. Ros, M. Nikkhah, The role of tumor-stroma interactions on desmoplasia and tumorigenicity within a microengineered 3D platform, Biomaterials 247 (2020), 119975.
[28] H.Y. Tanaka, T. Kurihara, T. Nakazawa, M. Matsusaki, A. Masamune, M.R. Kano, Heterotypic 3D pancreatic cancer model with tunable proportion of fibrotic elements, Biomaterials 251 (2020), 120077.
[29] C. Lodillinsky, L. Fuhrmann, M. Irondelle, O. Pylypenko, X.Y. Li, H. Bonsang-Kitzis, F. Reyal, S. Vacher, C. Calmel, O. De Wever, I. Bieche, M.L. Lacombe, A.M. Eijan, A. Houdusse, A. Vincent-Salomon, S.J. Weiss, P. Chavrier, M. Boissan, Metastasis-suppressor NME1 controls the invasive switch of breast cancer by regulating MT1-MMP surface clearance, Oncogene 40 (23) (2021) 4019–4032.
[30] Y. Shi, M.N. Simmons, T. Seki, S.P. Oh, S.P. Sugrue, Change in gene expression subsequent to induction of Pnn/DRS/memA: increase in p21(cip1/waf1), Oncogene 20 (30) (2001) 4007–4018.
[31] E.S. Knudsen, R. Nambiar, S.R. Rosario, D.J. Smiraglia, D.W. Goodrich, A.K. Witkiewicz, Pan-cancer molecular analysis of the RB tumor suppressor pathway, Commun. Biol. 3 (1) (2020) 158.
[32] J. Whitehead, K.H. Griffin, M. Gionet-Gonzales, C.E. Vorwald, S.E. Cinque, J.K. Leach, Hydrogel mechanics are a key driver of bone formation by mesenchymal stromal cell spheroids, Biomaterials 269 (2021), 120607.
[33] A. Bauer, L. Gu, B. Kwee, W.A. Li, M. Dellacherie, A.D. Celiz, D.J. Mooney, Hydrogel substrate stress-relaxation regulates the spreading and proliferation of mouse myoblasts, Acta Biomater. 62 (2017) 82–90.
[34] O. Chaudhuri, L. Gu, M. Darnell, D. Klumpers, S.A. Bencherif, J.C. Weaver, N. Huebsch, D.J. Mooney, Substrate stress relaxation regulates cell spreading, Nat. Commun. 6 (2015) 6364.
[35] M. Darnell, S. Young, L. Gu, N. Shah, E. Lippens, J. Weaver, G. Duda, D. Mooney, Substrate stress-relaxation regulates scaffold remodeling and bone formation in vivo, Adv. Healthc. Mater. 6 (1) (2017).
[36] S. Nam, R. Stowers, J. Lou, Y. Xia, O. Chaudhuri, Varying PEG density to control stress relaxation in alginate-PEG hydrogels for 3D cell culture studies, Biomaterials 200 (2019) 15–24.
[37] F.A.A. Ruiter, F.L.C. Morgan, N. Roumans, A. Schumacher, G.G. Slaats, L. Moroni, V.L.S. LaPointe, M.B. Baker, Soft, dynamic hydrogel confinement improves kidney organoid lumen morphology and reduces epithelial-mesenchymal transition in culture, Adv. Sci. 9 (20) (2022), e2200543.
[38] S. Phuagkhaopong, L. Mendes, K. Muller, M. Wobus, M. Bornhauser, H.V.O. Carswell, I.F. Duarte, F.P. Seib, Silk hydrogel substrate stress relaxation primes mesenchymal stem cell behavior in 2D, ACS Appl. Mater. Interfaces 13 (26) (2021) 30420–30433.
[39] S. Haque, J.C. Morris, Transforming growth factor-β: a therapeutic target for cancer, Hum. Vaccines Immunother. 13 (8) (2017) 1741–1750.
[40] T. Li, M.E. Forbes, G.N. Fuller, J. Li, X. Yang, W. Zhang, IGFBP2: integrative hub of developmental and oncogenic signaling network, Oncogene 39 (11) (2020) 2243–2257.
[41] S. Gao, Y. Sun, X. Zhang, L. Hu, Y. Liu, C.Y. Chua, L.M. Phillips, H. Ren, J.B. Fleming, H. Wang, IGFBP2 activates the NF-κB pathway to drive epithelial–mesenchymal transition and invasive character in pancreatic ductal adenocarcinoma, Cancer Res. 76 (22) (2016) 6543–6554.
[42] L. Sun, X. Zhang, Q. Song, L. Liu, E. Forbes, W. Tian, Z. Zhang, Y.a. Kang, H. Wang, J.B. Fleming, IGFBP2 promotes tumor progression by inducing alternative polarization of macrophages in pancreatic ductal adenocarcinoma through the STAT3 pathway, Cancer Lett. (Amsterdam, Neth.) 500 (2021) 132–146.
[43] H. Yamamoto, F. Itoh, S. Iku, Y. Adachi, H. Fukushima, S. Sasaki, M. Mukaiya, K. Hirata, K. Imai, Expression of matrix metalloproteinases and tissue inhibitors of metalloproteinases in human pancreatic adenocarcinomas: clinicopathologic and prognostic significance of matrilysin expression, J. Clin. Oncol. 19 (4) (2001) 1118–1127.